Ground impact probability distribution for small unmanned aircraft in ballistic descent

La Cour-Harbo, Anders

Published in:
2020 International Conference on Unmanned Aircraft Systems (ICUAS)

DOI (link to publication from Publisher):
10.1109/ICUAS48674.2020.9213990

Publication date:
2020

Document Version
Early version, also known as pre-print

Ground impact probability distribution for small unmanned aircraft in ballistic descent

Anders la Cour-Harbo
Department of Electronic Systems
Aalborg University
Fredrik Bajers Vej 7C, 9220 Aalborg East, Denmark
alc@es.aau.dk

***Abstract*—Safety is a key factor in all aviation, and while years of development has made manned aviation relatively safe, the same has yet to happen for unmanned aircraft. However, the rapid development of unmanned aircraft technology means that the range of commercial and scientific applications is growing equally rapid. At the same time the trend in national and international regulations for unmanned aircraft is to take a risk-based approach, effectively requiring risk assessment for every flight operation. This work addresses the growing need for methods for quantitatively evaluating individual flights by modelling the consequences of a ballistic descent of an unmanned aircraft as a result of a major in-flight incident. The presented model is a probability density function for the ground impact area based on a second order drag model with probabilistic assumptions on the least well-known parameters of the flight, and includes the effect of wind. The model has low computational complexity and is well-suited for high fidelity simulations for longer flights over populated areas and with changing trajectory parameters.**

I. Introduction

The reliability of small, commercially available civilian unmanned aircraft is, both from a components view and a systemic view, largely of aleatory nature, without much effort invested by technology developers and manufacturers in providing any form of guarantees on reliability or dependability. While the reliability arguably is increasing with each new generation of unmanned aircraft, we are still a long way from reaching a level equivalent to manned aviation. Consequently, the primary risk mitigation comes from temporal and/or spacial segregation. This is manifested in well-known regulatory constraints such as requiring flight to be not over people, away from roads, below a certain (low) altitude, and in particular, not beyond visual line-of-sight (BVLOS).

Such restrictions are generally a result of regulation authorities erring on the side of cautions rather than a result of a detailed quantitative analysis to determine to what extend current drone technology is endangering their operational environments. Therefore, there may be low hanging fruit to be picked by examining more carefully the risk associated with individual specific operations of unmanned aircraft. This is because some types of operations may indeed, despite being prohibit by regulation, have an associated risk that inherently and demonstrably is at the equivalent level of safety to manned aviation (or indeed some other level appropriate for the operation at hand) without resorting to certified and very costly technology.

The development of methods for quantifying the risk associated with a particular flight can to a large extend be based on existing methods from manned aviation accompanied by knowledge from other mature fields. The aim is to develop methods for the enhancement of the safety and reliability of unmanned aircraft and as for any complex technological system general methods of quantifying reliability are necessarily composed of numerous modules, and this work presents a model that contributes to one of them. In addition the lack of data from actual flights means that such methods must have a probabilistic component to account for both model and parameters uncertainties.

In aviation a classic measure of risk is fatalities per flight hour, which is practical in the sense that it compares well to other familiar risks such as driving a car or working in a dangerous environment. Additionally, substantial data is available for many such fields allowing for comparable and reasonable quantitative targets to be set for operations of unmanned aircraft.

In this work the focus is on one component for said quantitative analysis. In the event of (near) complete loss of lift an aircraft enters a ballistic descent trajectory and eventually impacts the ground with possible human injury as a consequence. Being able to predict the probability of impact is a key component in a risk analysis.

A. Background

The technology of unmanned aircraft has reached a level where many useful and commercially viable flights can be carried out with ease. Endurance is increasing to hours and even days, camera technology is sufficiently good to allow for commercial recordings, a plethora of remote and in-situ sensors are being miniaturized and automated. Unfortunately, the safety associated with operations of unmanned aircraft is not developing equally rapidly, and in particular the knowledge on the risks is not growing equivalently. This despite the fact that modern aviation regulation for unmanned aircraft is risk-based in the sense that main metric for limiting flights is the risk they pose, a policy that is clearly state in as

examples UK [33], Danish [28], and European [15] as well as industry [27] documents. In particular, the Implementing Act and Delegated Act [16] which implements the Specific category for risk-based operations is noteworthy. This work adhere to these policies by contributing to the risk assessment that naturally compliments the risk-based approach.

1) Background of present work: As part of the regulatory process in Denmark the Danish Transport, Construction and Housing Authority decided in early 2016 to initiate a project called BVLOS FastTrack to investigate what requirements and circumstances would be appropriate in order to grant (initially) a few companies permission to routinely conduct BVLOS operations in Danish airspace. At that time no permissions had been granted for BVLOS flight in Denmark except for flights in Greenland and individual flights confined to specific routes and dates. The purpose of the project was to grant permissions based on a thorough and scientific analysis of the risks involved for a range of BVLOS flights rather than just one specific flight. Danish UAS operator companies were invited to participate in the project, and their contribution would be supplying all information required for a thorough analysis as well as conducting a number of test flights to demonstrate the ability to adhere to proper procedures. In turn they would be, should the risk of their proposed BVLOS flight be acceptable, granted permission to conduct BVLOS operations within given limitations. The incitement would be that these limitation would not be specifically geographical and temporal, meaning that a flight permission would state that any flight within the given limits would be permitted independent of geographical location and point in time.

The concept of a risk-based approach has at the time of publishing this work been fully implemented by the SORA (Specific Operations Risk Assessment) set of documents [22], which provides an in-depth procedure for conducting a risk assessment for both the ground and air risk associated with specific types of operations. The SORA is primarily based on a rather coarse quantitative approach using tables for classification of risk, and work is ongoing to produce a new version of the SORA that adopts quantitative measures allowing for more graduated, and consequently (and hopefully) more accurate assessments.

The aim of this work is to address this specific need by developing a method that allows for immediate quantification of the risk for people on the ground when an unmanned aircraft flies overhead and suffers structural disintegration, leading to a ballistic descent. It should be noted that there are several other types of unintended descent of an aircraft, including gliding, fly-away, parachute, etc. which are not the subject of the present work.

B. Previous work

There are numerous works on how to conceptually approach the challenge of determining the risk of an unmanned aircraft flight. Much is borrowed from the world of manned aviation that has been conducting risk management for decades. A number of examples of risk assessments and quantifications for unmanned aircraft are the following. [9] addresses the lack of an accepted framework and provides some guidelines for how to apply existing models to manage the risk. [8] provides a comprehensive description of how to manage the risk of unmanned aircraft operations along with a series of quantification of existing risks for various types of aviation. Metrics for safety, including hazard metrics and risks metrics are presented in [26], in [14] a software safety case is developed, and in [13] a generic safety case is presented based on experience with NASA unmanned aircraft missions.

1) Ballistic trajectory analysis: A ballistic trajectory represents the motion of an object where the only major force acting on the object is gravity. This motion is easily described used Newtonian mechanics and the resulting differential equations are easily solved analytically. However, any object moving in the atmosphere is subjected to an aerodynamic force, often separated in to lift force and drag force, where for a ballistic trajectory the lift force is by definition small or vanishing. Adding a drag term to the differential equations makes it more complicated to obtain a solution, though. Most literature assumes a second order drag model similar to the one used here. Since such a model (in the general formulation) does not have an analytic solution most work in the field of ballistic trajectory analysis focus on numerical solutions. That includes all of the references in the following subsections.

Ballistic trajectories for a wide range of objects has been studied and analyzed for decades, and there is a significant amount on literature on the subject. In particular, descent of debris-like objects from aircraft accidents are closely related to the topic of this work. A basic review of the differential equations governing a standard second order drag model for aircraft debris scenarios is presented in numerous sources, including [19], [30], [23], [10]. A thorough description of debris footprint and how to determine it is found in [17], where a probabilistic approach with normal distributions is suggested for difficult to determine parameters such as drag coefficient and wind. This reference also has a detailed analysis of drag forces on debris.

2) Unmanned aircraft ground impact: The uncontrolled descent of unmanned aircraft into populated areas have been the subject in a number of publications. This includes [24] that investigate larger aircraft through an equivalent level of safety analysis. [40] specifically looks at distribution of possible impact locations based on simulation, and [6] uses a standard statistical setup and applies a normal distribution approach using aircraft glide parameters to model the impact location. In [4] a study for ground impact fatalities resulting from power failure and subsequent uncontrolled glide is presented. An study on the impact area for a general uncontrolled descent, including a buffer zone, is presented in [21]. A method for automatically finding a proper landing area for an aircraft in emergency descent is shown in [38], [37], and the ability of a fixed wing aircraft to glide to a designated emergency landing area is presented in [11]. In [2] a method for determining a no-thrust flight trajectory to reach a particular landing spot is presented. The barrier bow

tie model also used in manned aviation risk assessment is presented in [7]. A more high level review of risk metrics for unmanned aircraft is presented in [26]. A study of trajectory models for explosive debris [35] attempts to determine the impact point based on initial conditions.

Probabilistic modelling of ground fatalities for manned aviation has been studied, example are [34], [18], [32], but typically such research takes a somewhat different modelling approach due to the size of the aircraft, the typical flight altitude, etc. The idea of crash zones dependent on the characteristics of the aircraft and flight parameters for manned aviation is discussed in [12], [31]. The concept of area-based risk of fatalities from major incidents has also been studied in numerous context, one example from Germany is [5]. Finally, for a general introduction to probabilistic risk analysis, a good reference is [3].

As a side note; some work has been done on the consequences of small drones impacting humans. Most notably the UAS Ground Collision Severity Evaluation [1] studies the consequences of human drone impacts and includes parameters such as impact speed and impact angle, which can easily be derived from most descent models, including the model in present work.

3) Actual ballistic descents of manned aircraft: A ballistic descent of a structurally disintegrated Boeing 747 happened in May 2002 over Taiwan Strait when the aft fuselage structure of flight CI611 separated at 35.000 ft. The descent is modelled in [20] with standard second order drag model to generate the dynamic equations and with known wind patterns to account for the effect of wind during the descent. The modelling is found to be consistent with radar tracks as well as recorded salvage positions to a horizontal accuracy better than 1.000 ft.

The NTSB studied the ballistic descent of pieces of a TWA800, a Boeing 747 that broke up over the Atlantic Ocean in July 1996, using also a standard drag model and differential equations to model the dynamics [39]. An 'estimated ... range of values for the airplane's aerodynamic characteristics' were used, since the actual values were not known for the disintegrated aircraft. Wind data from a radiosonde balloon was interpolated to generate the wind effect for the descent [29].

C. Present work

The assumptions made in existing literature on the uncontrolled descent of small unmanned aircraft are typically quite crude in the sense that they do not account for different types of ways that an unmanned aircraft can experience such a descent, even though, say, ballistic and gliding descents arguably have very different consequences. A standard approach is to assume a normal (or similar) distribution of the impact point on the ground. As is evident from the method and results presented below this is a very coarse estimation at best. In addition, most works on ballistic descent assume a decoupling between the vertical and horizontal motions in order to reduce complexity of the solution. This rather simplifying assumption, as we show, is not necessary for a useful closed-form solution. This work contributes to the state of the art in two ways:

1) It provides a method for producing a georeferenced 2D probabilistic density function for the impact of a drone in ballistic descent, with appropriate stochastic assumptions to account for the modelling and parameters uncertainties.
2) It provides a closed-form solution to the coupled 2D dynamic ODEs governing the descent. This reduces the computational burden of conducting calculations for an entire flight by a three order of magnitude. Conducting a high fidelity computation for an entire flight will require many thousands, and most likely millions of ballistic descents. This will be cumbersome and inflexible to do by solving the coupled ODEs every time.

In the combination with descent models for loss of power, fly-away and other types of flight terminating events the modelling in this paper can be used for quantifying the total risk for a given flight. This allows operators to systematically have a safety assessment of each flight, either for the purpose of adhering to flight regulation or flight restrictions, or to form the basis for a application for dispensation when existing regulation does not allow a particular type of flight, such as BVLOS. The use of the ballistic descent model is exemplified in [25] to evaluate the risk of a power line inspection BVLOS flight operation with a Talon model aircraft.

II. Ballistic descent

The primary forces acting on a body in ballistic descent are gravity and drag force. A very standard model of the latter for speeds and shapes realistic for a crippled, descending aircraft is a second order model, i.e. the drag force is proportional to the square of the speed. Obviously, the drag force is the same for motions in any direction, even though we tend to consider the ballistic motion as decomposed into horizontal and vertical motions. In the method below a compromising semi-decoupling assumption is made that allows for a closed-form solution as well as a solution close to the solution of the fully coupled 2D dynamic equations.

A. Ballistic drop quadratic drag model

The standard second order model for ballistic descent with drag takes the following form

$$m\dot{\mathbf{v}} = m\mathbf{g} - c|\mathbf{v}|\mathbf{v} \ , \tag{1}$$

where m is aircraft mass and c is a constant that captures the drag coefficient, drag area, and air density. Here we will focus on the 2D version where the vectors exist in a vertical plane spanned by the horizontal flight direction and direction of gravity. A standard assumption in most previous work, including most of the references above, is that this equation can be separated into horizontal and vertical motion without coupling

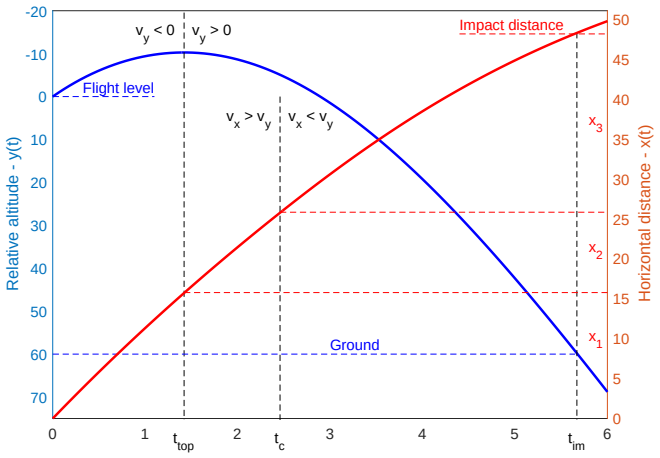

Fig. 1. The y (blue) and x (red) show the position trajectories for a descent according to the ODEs in (2) and (3). The horizontal axis is time. See text for further explanation.

Since (1) does not appear to have analytic solutions for arbitrary boundary conditions, we look at the following problem instead. We will assume that $v_x > 0$ and monotonically decreasing as there is no thrust force in the horizontal plane to affect the aircraft. We will also assume that v_y will asymptotically approach the velocity where gravity and drag force cancel out. Consequently, the following model is a reasonably good approximation to (1)

$$m\dot{v}_x = -c\max(v_x, v_y)v_x \tag{2}$$
$$m\dot{v}_y = mg - c|v_y|v_y \ . \tag{3}$$

The first equation described the horizontal motion, where there is no gravity. Initially, the horizontal velocity is dominating. Over time it will decreased monotonically, while the vertical will increase monotonically. Consequently, there will be a single point in time where the vertical speed is "more important" than the horizontal speed. This happens when $v_x = v_y$, and therefore (2) uses the maximum as an approximation to decoupled the equations for the later part of the descent.

The second equation (3) describes the vertical motion, where the coupling to v_x has been left out altogether, because v_x decreased relatively quickly initially, and thus have little influence of the vertical motion for the majority of the descent trajectory.

The resulting position trajectory for y and x will be shaped as seen in Figure 1. This figures shows how the motion changes phase twice during the descent at times t_{top} (caused by the absolute value in (3)) and t_{c} (caused by the maximum in (2)). The impact occurs at time t_{im}. This descent in Figure 1 has parameters: Ground at $y = 60$, $m = 5$, $c = 0.052$, $v_{y,\text{i}} = -15$, and $v_{x,\text{i}} = 12$. Variables x_1, x_2, and x_3 represent the horizontal distances traveled during the three phases.

With the initial condition $v_x(0) = v_{x,\text{i}}$ and $v_y(0) = v_{y,\text{i}}$ the horizontal air velocity is then given as

$$v_x(t) = \begin{cases} \dfrac{mv_{x,\text{i}}}{m + v_{x,\text{i}}ct} & v_x > v_y \quad (4) \\ v_{x,\text{i}} \exp\Big(-\dfrac{c}{m}\displaystyle\int_0^t v_y(\tau)d\tau\Big) & v_x \le v_y \quad (5) \end{cases}$$

and the vertical velocity as

$$v_y(t) = \begin{cases} \Gamma\tan\big(g\gamma t + H_{\text{u}}\big) & v_y(t) < 0 \quad (6) \\ \Gamma\tanh\big(g\gamma t + H_{\text{d}}\big) & v_y(t) \ge 0 \quad (7) \\ \Gamma & v_y(0) = \Gamma \quad (8) \end{cases}$$

$$H_{\text{d}} = \operatorname{arctanh}(v_{y,\text{i}}\gamma) \quad \text{and} \quad H_{\text{u}} = \arctan(v_{y,\text{i}}\gamma) \ ,$$

where $\Gamma = \sqrt{mg/c}$ is the terminal velocity (gravitational force and drag force are equal with opposite signs) and $\gamma = 1/\Gamma$. The case (8) is for the situation where the initial vertical velocity is equal to the terminal velocity and (7) therefore is undefined (since $H_{\text{d}} = \operatorname{arctanh}(1)$ is undefined). Typically, $c = 0.5\rho A C_{\text{D}}$, where ρ is the air density, A is the frontal area, and C_{D} the drag coefficient. Note that H_{d} is complex for $v_{y,\text{i}} > \Gamma$.

The ballistic trajectory of the aircraft may start with an upwards motion where $v_y(t) < 0$, and will always end with a downward motion. From (6) it follows that the transition occurs at time

$$t_{\text{top}} = -\frac{\Gamma}{g}H_{\text{u}} \ ,$$

which is negative (and thus not occurring in the descent) when $v_{y,\text{i}} \ge 0$. The horizontal motion is always positive in this setup.

The traversed vertical distance can be found for the downward and upward motions by integration $\int_0^t v_y(w)dw$, which gives

$$y_{\text{u}}(t) = -\frac{m}{c}\Big(\ln\big(\cos(g\gamma t + H_{\text{u}})\big) - G_{\text{u}}\Big) \tag{9}$$
$$y_{\text{d}}(t) = \ \frac{m}{c}\Big(\ln\big(\cosh(g\gamma t + H_{\text{d}})\big) - G_{\text{d}}\Big) \tag{10}$$

where

$$G_{\text{u}} = \ln\cos H_{\text{u}} = -\frac{1}{2}\ln\big(1 + (v_{y,\text{i}}\gamma)^2\big) \ , \tag{11}$$
$$G_{\text{d}} = \ln\cosh H_{\text{d}} = -\frac{1}{2}\ln\big(1 - (v_{y,\text{i}}\gamma)^2\big) \ . \tag{12}$$

Note that G_{d} becomes complex for $v_{y,\text{i}} > \Gamma$.

For $v_{y,\text{i}} \ge 0$ the drop time from a given flight altitude y can be found from (10) to be

$$t_{\text{drop}}(y) = \Big(\operatorname{arccosh}\Big(\exp\Big(\frac{cy}{m} + G_{\text{d}}\Big)\Big) - H_{\text{d}}\Big)\frac{\Gamma}{g} \ , \tag{13}$$

and the total time from event to impact can be found as

$$t_{\text{im}}(y) = \begin{cases} t_{\text{top}} + t_{\text{drop}}\big(y + y_{\text{u}}(t_{\text{top}})\big)\big|_{H=G=0} & v_{y,\text{i}} < 0 \\ t_{\text{drop}}(y) & v_{y,\text{i}} \ge 0 \end{cases}$$

To find the horizontal distance traversed we first need to determine the time at which $v_x(t) = v_y(t)$. Since $v_x > 0$ the equality is for $v_y(t) > 0$, so we use (4) and (7) in the equation. Since an equation on the form $\tanh(at) = 1/t$ does not appear to have a closed form solution we will use a

truncation of the continued fraction for the hyperbolic tangent function to approximate the point in time where $v_x(t)$ goes from (4) to (5). That is

$$\begin{aligned} v_y(t - t_{\text{top}}) &\approx \frac{g\gamma(t - t_{\text{top}}) + H_{\text{d}}}{1 + \big(g\gamma(t - t_{\text{top}}) + H_{\text{d}}\big)^2} \\ &= \frac{mv_{x,\text{i}}}{m + v_{x,\text{i}}ct} = v_x(t) \ . \end{aligned}$$

This formulation cover both positive and negative $v_{y,\text{i}}$; for $v_{y,\text{i}} < 0$ we set $H_{\text{d}} = 0$ and for $v_{y,\text{i}} \geq 0$ we set $t_{\text{top}} = 0$. In any case this only has one solution despite the appearance of a second order equation, which becomes evident as the coefficient for the second order term is zero. Thus, the solution is the negative fraction between the zeroth and first order coefficients, which reduces to

$$t_{\text{c}} = \frac{m(gt_{\text{top}} - \Gamma H_{\text{d}} + v_{x,\text{i}}(1 + (H_{\text{d}} - g\gamma t_{\text{top}})^2)}{mg + cv_{x,\text{i}}(gt_{\text{top}} - \Gamma H_{\text{d}})} \ , \quad (14)$$

where subscript c is short for 'crossing from v_x to v_y'. Since the truncated fraction is an approximation of $\tanh(x)$ around $x = 0$, and since the fraction has an asymptote in 0 the approximated solution tends to be larger than the true solution (which can easily be found numerically with a gradient search or similiar, since the functions involved are monotonic).

The traversed horizontal distance can now be found by first noting that (5) can be written as

$$\begin{aligned} v_x(t) &= v_{x,\text{i}} \exp\Big(-\frac{c}{m} y_{\text{d}}(t)\Big) \quad (15) \\ &= v_{x,\text{i}} e^{G_{\text{d}}} \operatorname{sech}(g\gamma t + H_{\text{d}}) \ . \quad (16) \end{aligned}$$

Then integration gives

$$x_{v_x}(t) = \frac{m}{c} \ln(1 + v_{x,\text{i}}ct/m) \quad (17)$$

for $t \leq t_{\text{c}}$ and

$$\begin{aligned} x_{v_y}(t) = \frac{v_{x,\text{i}} e^{G_{\text{d}}} \Gamma}{g} \Big(&\arctan\big(\sinh(g\gamma t + H_{\text{d}})\big) \\ &- \arcsin(v_{y,\text{i}}\gamma)\Big) \quad (18) \end{aligned}$$

for $t > t_{\text{c}}$.

Four examples of velocities are shown in Figure 2, and the position trajectories for the first of the four examples are the ones shown in Figure 1. Figure 2 shows graphs for numerical solutions to (1). The initial velocities and masses are shown above each plot. Additionally, $g = 9.82$, $\rho = 1.3$, $A = 0.1$, and thus $c = 0.052$. Note that the y axis is 'reversed' in relation to $v_y(t)$.

B. Traveled distance before impact

The goal of this paper is to find the horizontally traveled distance from the point of incidence to the ground impact point. With the equations derived in the previous section this can now be done in the following way. If $t_{\text{im}}(y) \leq t_{\text{c}}$ the distance simply becomes

$$x(y) = x_{v_x}(t_{\text{im}}(y)) \ . \quad (19)$$

However, if $t_{\text{im}}(y) > t_{\text{c}}$ then

$$x(y) = x_{v_x}(t_{\text{c}}) + x_{v_y}(t_{\text{im}}(y) - t_{\text{top}})\Big|_{\substack{v_{x,\text{i}} = v_x(t_{\text{c}}) \\ v_{y,\text{i}} = v_y(t_{\text{c}})}} \quad (20)$$

where the second part of the travel, given by x_{v_y}, must use the appropriate initial velocities.

C. Actual calculations

In order to actually compute the horizontally traveled distance one of two approaches can be used; either use a number of conditional statements to distinguish the various combinations, or modify some of the variables during computations to accommodate the various combinations. The former would require less computation, while the latter is suitable for a vector implementation, in say Matlab. Since the former is largely covered in the previous derivations we will here show the latter implementation method.

In the following some of the variables may have value 0 for some input values (for instance $t_{\text{top}} = 0$ when $v_{y,\text{i}} \geq 0$), and to differentiate such cases from the variables in the previous section we use the hat symbol. Now, first, define

$$\hat{v}_{y,\text{i}} = \max(0, v_{y,\text{i}})$$

and integral initial conditions

$$\begin{aligned} \hat{H}_{\text{d}} &= \operatorname{arctanh}(\hat{v}_{y,\text{i}}\gamma) \ , \\ \hat{H}_{\text{u}} &= \arctan(\hat{v}_{y,\text{i}}\gamma) \ , \\ \hat{G}_{\text{d}} &= \ln\cosh \hat{H}_{\text{d}} \ , \\ \hat{G}_{\text{u}} &= \ln\cosh \hat{H}_{\text{u}} \ . \end{aligned}$$

The time the aircraft is at highest altitude is

$$\hat{t}_{\text{top}} = -\frac{\Gamma}{g} \arctan\big(\gamma \min(0, v_{y,\text{i}})\big) \ . \quad (21)$$

The horizontal distance traveled for reaching highest altitude is

$$x_1 = x_{v_x}(\hat{t}_{\text{top}}) \ .$$

The time of crossing the point where $v_x = v_y$ is

$$\hat{t}_{\text{c}} = t_{\text{c}}(\hat{t}_{\text{top}}, \hat{H}_{\text{d}}) \ .$$

The altitude gained from flight level to highest altitude is

$$y_{\text{top}} = y_{\text{u}}(\hat{t}_{\text{top}}) = -\frac{m}{2c} \ln\big(1 + (\gamma \min(0, v_{y,\text{i}}))^2\big) \ .$$

The time is takes to descent from highest altitude to ground impact is

$$\hat{t}_{\text{drop}} = t_{\text{drop}}(y - y_{\text{top}}, \hat{H}_{\text{d}}, \hat{G}_{\text{d}})$$

and the total time from event to impact is

$$\hat{t}_{\text{im}} = \hat{t}_{\text{top}} + \hat{t}_{\text{drop}} \ . \quad (22)$$

The horizontal velocity at highest altitude is

$$v_{x,\text{top}} = v_x(\hat{t}_{\text{top}}) = \frac{mv_{x,\text{i}}}{m + v_{x,\text{i}}c\hat{t}_{\text{top}}} \ .$$

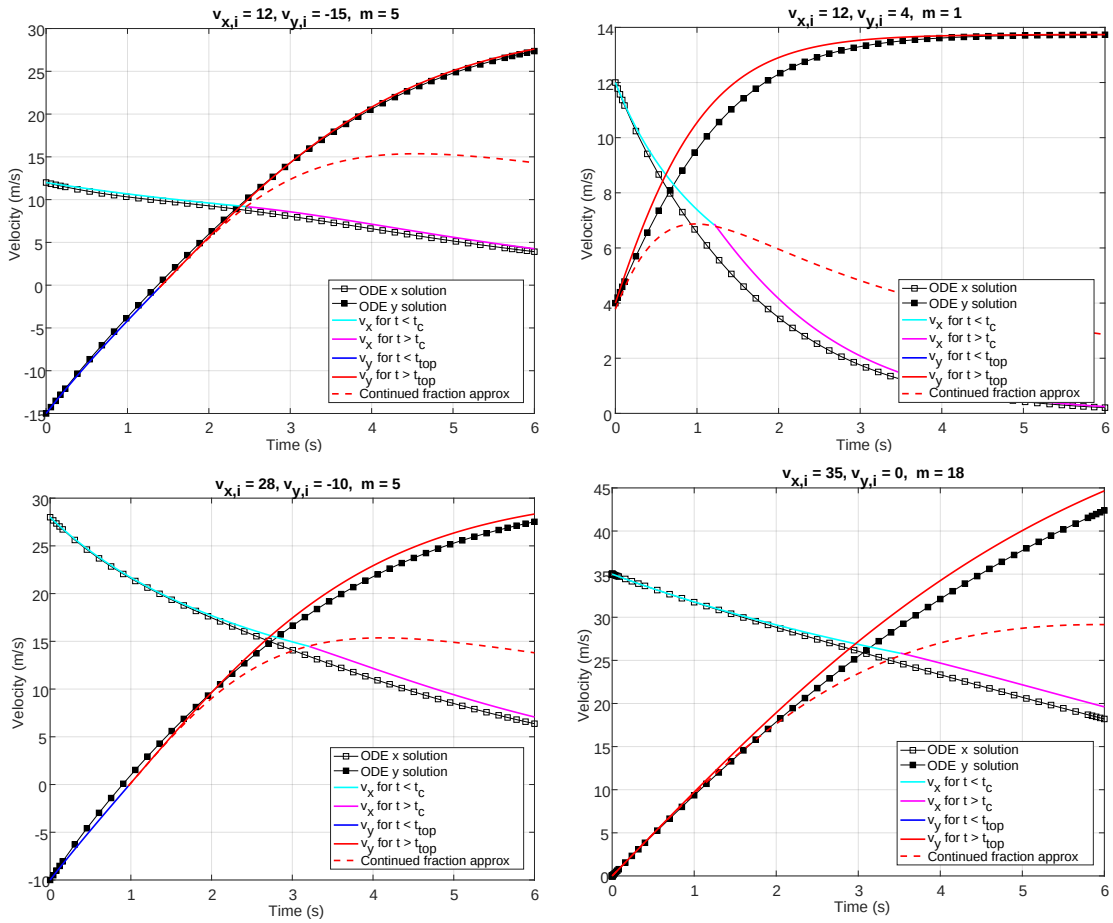

Fig. 2. Four examples of using (4) and (15) for $v_x(t)$, and (6) and (7) for $v_y(t)$. The ODE solutions are the solutions to (1). See text for further details.

The horizontal distance traveled from highest altitude to the point where $v_x = v_y$ is then

$$x_2 = x_{v_x}\big(\min(\hat{t}_{\rm im}, \hat{t}_{\rm c}) - \hat{t}_{\rm top}\big)\Big|_{v_{x,\rm i}=v_{x,\rm top}}$$
$$= \frac{m}{c}\ln\Big(1 + cv_{x,\rm top}\frac{\min(\hat{t}_{\rm im}, \hat{t}_{\rm c}) - \hat{t}_{\rm top}}{m}\Big)$$

The horizontal and vertical velocities at the time of crossing are (in fact not the same, since the crossing time is approximated)

$$v_{x,\rm c} = v_x(\hat{t}_{\rm c}) = \frac{mv_{x,\rm i}}{m + v_{x,\rm i}c\hat{t}_{\rm c}}\ ,$$
$$v_{y,\rm c} = v_y(\hat{t}_{\rm c} - \hat{t}_{\rm top}) = \Gamma\tanh\Big(g\gamma(\hat{t}_{\rm c} - \hat{t}_{\rm top}) + \hat{H}_{\rm d}\Big)\ .$$

In order to compute the last part of the trajectory it is convenient with the following definition

$$H_{\rm c} = \operatorname{arctanh}(\gamma v_{y,\rm c}) \quad \text{and} \quad G_{\rm c} = \ln\cosh H_{\rm c}\ .$$

The horizontal distance traveled from the point where $v_x = v_y$ to the impact point is then

$$x_3 = \frac{v_{x,\rm c}e^{G_{\rm c}}\Gamma}{g}\Big(\arctan\big(\sinh(g\gamma t + H_{\rm c})\big)$$
$$- \arcsin(\gamma v_{y,\rm c})\Big)\ .$$

The total traveled horizontal distance from event point projected onto the ground to impact point is then

$$x = x_1 + x_2 + x_3\ . \tag{23}$$

The impact velocity can now be computed as

$$v_{x,\rm im} = \begin{cases} \dfrac{mv_{x,\rm i}}{m + v_{x,\rm i}c\hat{t}_{\rm im}} & \hat{t}_{\rm im} \le \hat{t}_{\rm c} \\ v_{x,\rm c}e^{G_{\rm c}}\operatorname{sech}\Big(g\gamma(\hat{t}_{\rm im} - \hat{t}_{\rm c}) + H_{\rm c}\Big) & \hat{t}_{\rm im} > \hat{t}_{\rm c} \end{cases}$$

and as

$$v_{y,\rm im} = \Gamma\tanh\Big(\frac{g}{\Gamma}(\hat{t}_{\rm im} - \hat{t}_{\rm top}) + \hat{H}_{\rm d}\Big)\ .$$

D. Simplified versions

With a few assumptions this can be simplified somewhat. Assume $v_{{\rm i},y} = 0$ and using $\operatorname{arccosh}(x) = \ln(x + \sqrt{x^2 - 1})$ for $x > 1$ we can rewrite (13) for $cy > m$ as

$$t_{\rm drop}(y) = \left(\ln\Big[\exp\Big(\frac{cy}{m}\Big) + \sqrt{\exp\Big(\frac{cy}{m}\Big)^2 - 1}\Big]\right)\frac{\Gamma}{g}$$
$$\approx \Big(\ln 2 + \frac{cy}{m}\Big)\frac{\Gamma}{g}$$
$$= \frac{(m\ln 2 + cy)\Gamma}{mg}$$

where the approximation is good for $cy > m$, better than a factor

$$\frac{\ln(e+\sqrt{e^2-1})}{\ln 2+1} \approx 0.9789 \ ,$$

Thus, a good approximation to $x(y)$ as long as $t_{\rm im} < t_{\rm c}$ is

$$\tilde{x}(y) = \frac{m}{c}\ln\Big(1+v_{x,\rm i}\frac{m\ln 2+cy}{m\Gamma}\Big), \quad cy > m \ .$$

An alternative to the exact solution is to make the assumption that $v_x \gg v_y$ during the descent. This will be the case for high speed descent starting a low altitude. Then a good approximation to (1) is

$$m\dot{\mathbf{v}} = m\mathbf{g} - cv_x\mathbf{v} \tag{24}$$

where the solution for x is the same as (4) and (17), but for y becomes

$$v_y(t) = \frac{v_{\rm i,y}+gt/2}{1+at} + \frac{gt}{2} \ , \tag{25}$$

$$y(t) = \Big(v_{\rm i,y} - \frac{g}{2a}\Big)\frac{1}{a}\ln(1+at) + \frac{1}{4}gt^2 + \frac{gt}{2a} \ , \tag{26}$$

where $a = cv_{x,\rm i}/m$. As long as the angle deviation from horizontal is less than 20° this approximation is quite good [36].

III. Probability density function for traveled distance

The derivations done so far will for a given aircraft with given parameters predict one location of impact relative to the event location. While a descending aircraft will indeed impact at one location it is most likely not going to be at the predicted impact location, but rather somewhere near this location. Two of the main uncertainties contributing to this is uncertainty in drag force and uncertainty in the speed at the time of event. Making the assumption that these parameters are draw from known distributions the impact location becomes a probability density function that depends on the traveled distance from event location to impact location.

A. Uncertainties on drag coefficient and initial speed

The drag force, as expressed in (1), on the crippled aircraft is governed by c, which in turn depends on both the drag coefficient and the frontal area facing the travel direction. These parameters are inherently difficult to determine for an aircraft that may have lost an engine or a wing. To capture this uncertainty it is reasonable to assume that the drag coefficient is a stochastic parameter from a known distribution, while the frontal area is assumed to be given as some fraction of the aircraft frontal area as seen from the direction with the largest area. While it presumably would be more accurate to assume the frontal area as a stochastic parameter as well, the associated increase in computational complexity in determining the traveled distance PDF is not insignificant, while the added value of assuming stochastic properties of two multiplied parameters, albeit not vanishing, may still be close be negligible, given the overall uncertainty that we can expect in this scenario.

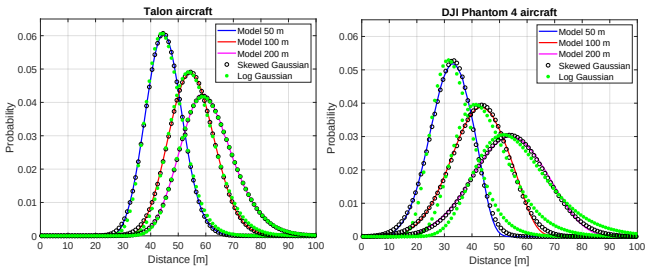

Fig. 3. Distribution of horizontal distance traveled for three different altitude and two different aircraft. See text for further details.

TABLE I
Parameters for the aircraft used as examples.

Spec	Phantom 4	Talon
Mass (kg)	1.4	3.75
Front area (m^2)	0.02	0.1
Drag coefficient	N(0.7,0.2)	N(0.9, 0.2)
Initial horizontal speed (m/s)	N(10,3)	N(18,3)
Initial vertical speed (m/s)	N(0,2)	N(0,4)

The velocity in (1) is presumably also not known exactly at the time of the event. For many flights a preplanned route is used, which typically includes a predetermine flight speed, which in turn allows for computing an expected velocity at any given point on the flight. However, due to uncertainties in airspeed measurement and due to the effect of the onboard controller attempting to maintain not just speed, but also altitude and heading, the actual velocity may easily vary somewhat from the expected value. These variations are very difficult to predict, and are therefore best handled by assuming that the initial velocity for an event is also a stochastic parameter. Since the horizontal and vertical speeds are separate in the above derivations the stochastic assumption is on both speeds.

If we assume that the drag coefficient and the initial horizontal and vertical speeds of the drone through the air is known only as a sample from normal distributions with given means and variances we can compute the resulting distribution on traveled distance by propagating the multivariate normal probability distributions through the appropriate equations and plotting the result. Some examples of this is shown in Figure 3. The parameters used for this examples are given in Table I. In Figure 3 the dots show approximations using least square best fit of skewed normal and log normal distributions. Parameters for these fits are shown in Table II.

B. Approximation with known distributions

The examples of traveled distance probability density functions in the previous section all seem to resemble known distributions, and it would arguably diminish the not insignificant computational effort involved in propagating the stochastic parameters through the model if it was possible to correlate the flight parameters to parameters of a known distribution. While determining such a correlation is beyond

TABLE II
PARAMETERS FOR THE FITTING OF SKEWED NORMAL DISTRIBUTION SHOWN IN FIGURE 3.

Aircraft	Altitude (m)	Skewed normal				Log normal		
		ξ	ω	α	C	μ	σ	C
Talon	50	38.3	9.06	2.03	1.01	3.79	0.139	1.01
	100	45.5	15.2	2.32	1.02	4.02	0.180	1.02
	200	48.0	26.5	3.48	1.03	4.19	0.247	1.02
Phantom	50	27.4	5.79	0.783	1.00	3.41	0.167	1.00
	100	35.3	8.49	1.02	1.00	3.69	0.174	1.00
	200	42.2	13.4	1.42	1.01	3.93	0.200	1.01

the scope of this work, we do want to note the similarity between the traveled distance PDFs and the skewed normal and log normal distributions.

The skewed normal distribution can be written on the form

$$\frac{2C}{\omega}\phi\Big(\frac{x-\xi}{\omega}\Big)\Phi\Big(\alpha\frac{x-\xi}{\omega}\Big)\ , \tag{27}$$

where ϕ and Φ are the normal PDF and the normal CDF with zero mean and unit variance, respectively. The log normal distribution can be written on the form

$$\frac{C}{x\sigma\sqrt{2\pi}}\exp\Big(\frac{-(\ln x-\mu)^2}{2\sigma^2}\Big)\ . \tag{28}$$

In Figure 3 both distributions have been fitted (in a least square sense) to the PDFs. For these examples the fitting parameters are shown in Table II. Note that since the curves are all PDFs they ideally have parameter $C = 1$. However, the assumption that both drag coefficient and initial speeds are normally distributed (and thus with infinite support) implies the assumption that there is a probability, albeit small, of a negative drag coefficient and negative initial speeds. These are disregarded in the computation resulting in a probability slightly less than 1, and thus scalings of the fitted functions of slightly more than 1.

IV. GROUND IMPACT PROBABILITY DENSITY FUNCTION

The derivation above to find the impact point happens in the 'air frame', that is, the aircraft travels at a given speed w and direction ψ relative to the air. Thus, the PDFs shown in Figure 3 are only valid for the inertia coordinate system if there is no movement of the air, that is, no wind. Additionally, since the air velocity is unlikely to be parallel to the flight direction adding the effect of the wind will change the ground impact location PDF from 1D to 2D, covering a geographical area rather than just a line segment.

A. Uncertainty in wind velocity

Assuming now that the air volume moves at a constant and horizontal speed and in a constant direction (independent of altitude and without turbulence) we can find the actual impact point during a ballistic descent simply by adding the horizontal translational motion of the aircraft with the air volume determined as the drop time times wind velocity. This will generally move the impact point away from the line coincident with the flight direction, thus introducing the possibility of impacting the ground away from the (straight) flight trajectory.

TABLE III
PARAMETERS FOR THE FOUR GRAPHS IN FIGURES 4 AND 5.

Plot	Aircraft	y	$\psi*$		w		θ
			μ	σ	μ	σ	
1	Talon	50	0	20	5	2	45
2	Talon	50	100	10	12	7	170
3	Phantom	150	190	60	9	2	90
4	Phantom	200	n/a	n/a	5.8	3	45

* Wind direction is given in degree with east as zero and positive counter-clockwise.

The impact point relative to the projection of the event point onto the ground becomes the vector

$$\mathbf{p}(y) = \begin{bmatrix}\cos\theta & -\sin\theta\\ \sin\theta & \cos\theta\end{bmatrix}\begin{bmatrix}x(y)\\ 0\end{bmatrix} + w\begin{bmatrix}\cos\psi\\ \sin\psi\end{bmatrix}t(y)\ , \tag{29}$$

where y is the altitude, ψ and w are wind direction and speed, θ the flight direction, and x and t are the traveled distance and drop time as given by (23) and (22), respectively. Depending on the circumstances the wind may or may not be known accurately, and it make sense to assume that both direction and speed are stochastic variables from distributions that reflects the knowledge one would have for a particular scenario. For computations just prior to flight, or even during flight, normal distributions for both direction and speed are presumably appropriate. For more generic computation a uniform distribution covering 2π rad for wind direction and a uniform distribution from 0 to maximum allowable wind speed (as given by specifications of the platform) would be a good choice. And a computation for a given geographical location could be based on actual historical data on the distribution of wind speed and direction for that particular location (when available).

Four examples of 2D PDFs for the ground impact points as given by (29) are shown in Figures 4 and 5. The distribution parameters for the four examples are given in Table III, while the aircraft parameters remains the same as previously. The plots are made by directly propagating sampled distributions through the model. Since the parameters are independent the covariance matrix is diagonal and the joint distribution is the product of the individual distributions, which in turn reduces the computational complexity. The second PDF in Figure 5 uses actual wind direction data from Karup Airport in Denmark rather than a normal or uniform distribution. The data used is average over 16 years (2001–2017), but may as easily be typical directional data from a given week or month (as the direction may change somewhat with changing seasons). The wind direction distribution is shown in Figure 6. The average wind speed is 5.8 m/s.

V. CONCLUSION

We have presented a method for determining the 2D geographical probability density function for the ground impact point for at ballistic descent with probabilistic assumptions on some of the aircraft parameters as well as the wind

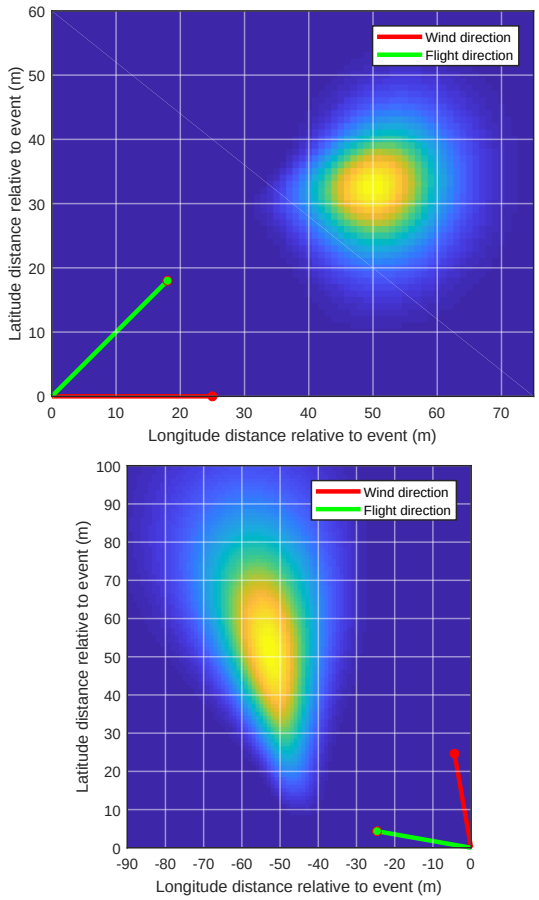

Fig. 4. PDF for two different parameter sets for the Talon aircraft. Ballistic descent starts at the origin. Parameters are found in Table I and III.

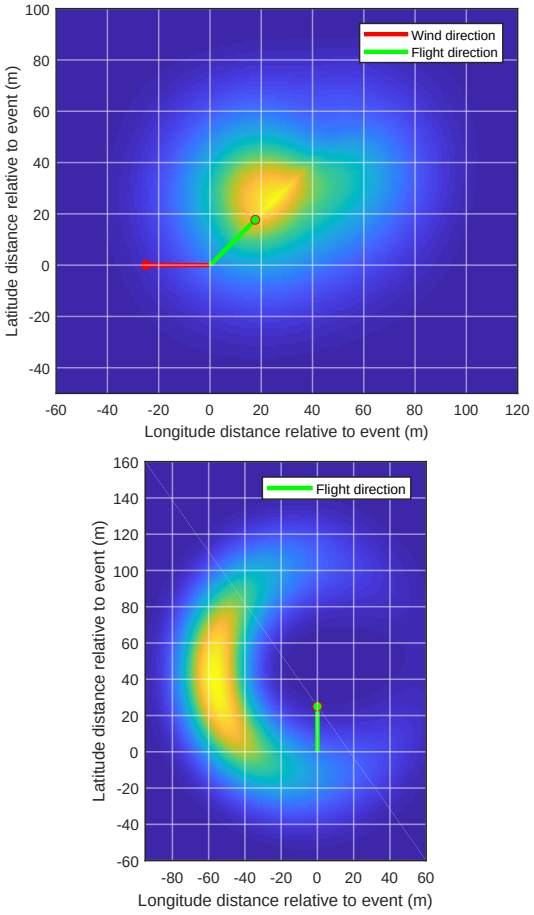

Fig. 5. PDF for two different parameter sets for the Phantom aircraft. Note that the last plot is based on actual wind data.

parameters. The method is basically a closed-form solution to the general ODEs of a 2D second order drag model, with simplifying assumptions for the particular case of a unpowered, gravity-driven ballistic descent. The resulting 2D PDF can be computed fast and is therefore suitable for application to the concept of sampling a longer flight trajectory over areas with varying population density and for varying flight parameters (such as aircraft altitude and velocity).

A. Application to quantitative risk assessment

The PDF presented here is a piece in a larger puzzle to achieve a quantitative risk assessment of a given unmanned aircraft operation. This assessment will ultimately be a fatality rate for the operation. The PDF is useful for determining the probabilities of impacting persons on the ground in the case of a ballistic descent, and this is done by correlation the georeferenced PDF with the associated person density for that particular geographical area. This can be done with varying fidelity depending on the availability of data; this can be population density at a coarse scale (as in most literature) or at a finer scale (Denmark has publicly available the latitude and longitude of all registered addresses in the country), or it can be designated areas where a high density is assumed

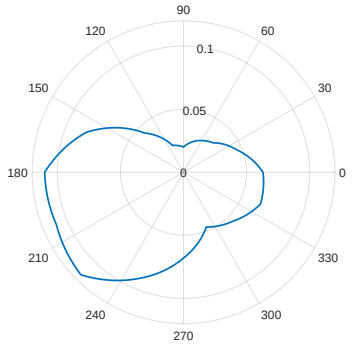

Fig. 6. Wind direction distribution for Karup Airport averaged over the period 2001 – 2017.

due to events (like concerts or festivals) or due to very busy areas like downtown metropolis and parks. Obviously, the ballistic descent is not the only flight terminating event that must be considered since an unmanned aircraft can descent uncontrolled in other ways, such as a glide due to lost power or a fly-away. Two examples of a complete calculation to achieve the flight fatality rate are given in [25] and [4].

An implementation of the descent model equations from Section II-C may be found in the CasEx python package.

ACKNOWLEDGMENT

This work is supported by the BVLOS FastTrack project, a cooperation between the Danish Traffic, Housing, and Construction Agency, University of Southern Denmark, Aalborg University, and Heliscope. It is also supported by the SafeEYE project grant no. 7049-00001 from Innovation Foundation Denmark.

REFERENCES

[1] David Arterburn, Mark Ewing, Raj Prabhu, Feng Zhu, and David Francis. FAA UAS Center of Excellence Task A4 : UAS Ground Collision Severity Evaluation. Technical report, ASSURE, 2017.

[2] Ella M. Atkins, Igor Alonso Portillo, and Matthew J. Strube. Emergency Flight Planning Applied to Total Loss of Thrust. *Journal of Aircraft*, 43(4):1205–1216, jul 2006.

[3] Tim Bedford and Roger Cooke. *Probabilistic Risk Analysis: Foundations and Methods*. Cambridge University Press, 2001.

[4] S Bertrand, N Raballand, F Viguier, and F Muller. Ground Risk Assessment for Long-Range Inspection Missions of Railways by UAVs. In *Proceedings of ICUAS 2017*, pages 1343–1351, 2017.

[5] D Borst, D Jung, S M Murshed, and U Werner. Development of a methodology to assess man-made risks in Germany. *Natural Hazards and Earth System Science*, 6(March):779–802, 2006.

[6] Reece Clothier, Rodney Walker, Neale Fulton, and Duncan Campbell. A casualty risk analysis for unmanned aerial system (UAS) operations over inhabited areas. In *Second Australasian Unmanned Air Vehicle Conference*, pages 1–15, 2007.

[7] Reece Clothier, Brendan Williams, and Achim Washington. Development of a Template Safety Case for Unmanned Aircraft Operations Over Populous Areas. In *SAE 2015 AeroTech Congress & Exhibition*, page 10, sep 2015.

[8] Reece A. Clothier and Rodney A. Walker. The Safety Risk Management of Unmanned Aircraft Systems. In Kimon P. Valavanis and George J. Vachtsevanos, editors, *Handbook of Unmanned Aerial Vehicles*, page 37. Springer Science + Business Media B.V., Dordrecht, Netherlands, 2013.

[9] Reece A. Clothier, Brendan P. Williams, and Neale L. Fulton. Structuring the safety case for unmanned aircraft system operations in non-segregated airspace. *Safety Science*, 79:213–228, 2015.

[10] J. D. Collins, M. Jameson, and J. L. Jantz. Real-time debris patterns for ballistic missile launches. *Journal of Spacecraft and Rockets*, 13(5):310–315, may 1976.

[11] Matthew Coombes, Wen-Hua Chen, and Peter Render. Landing Site Reachability in a Forced Landing of Unmanned Aircraft in Wind. *Journal of Aircraft*, pages 1–13, feb 2017.

[12] P.A. Davis and D.J. Quinn. Airport Public Safety Zones: Part 2 - Risk Model Application. In Cornelia Spitzer, Ulrich Schmocker, and Vinh N. Dang, editors, *Probabilistic Safety Assessment and Management - PSAM 7 - ESREL*, pages 242–247, 2004.

[13] Ewen Denney and Ganesh Pai. Architecting a Safety Case for UAS Flight Operations. In *34th International System Safety Conference*, page 12, 2016.

[14] Ewen Denney, Ganesh Pai, and Ibrahim Habli. Perspectives on software safety case development for unmanned aircraft. *Proceedings of the International Conference on Dependable Systems and Networks*, 2012.

[15] EASA. Opinion No 01/2018: Introduction of a regulatory framework for the operation of unmanned aircraft systems in the 'open' and 'specific' categories, 2018.

[16] EU. COMMISSION DELEGATED REGULATION (EU) .../... on unmanned aircraft systems and on third-country operators of unmanned aircraft systems, 2019.

[17] FAA. Flight Safety Analysis Handbook Federal Aviation Administration. Technical report, Federal Aviation Administration, sep 2011.

[18] Bernard D. Goldstein, Michele Demak, Mary Northridge, and Daniel Wartenberg. Risk to Groundlings of Death Due to Airplane Accidents: A Risk Communication Tool. *Risk Analysis*, 12(3):339–341, sep 1992.

[19] Matthew Greaves. Revisiting trajectory analysis - Evolving the Cranfield model. Technical report, safety and Accident Investigation Centre, Cranfield University, 2012.

[20] Wen-Lin Guan and Kay Yong. Ballistic Trajectory Analysis for the CI611 Accident Investigation. Technical report, Aviation Safety Council, Taipei, Taiwan, 2003.

[21] Giorgio Guglieri and Gianluca Ristorto. Safety Assessment for Light Remotely Piloted Aircraft Systems. In *2016 INAIR - International Conference on Air Transport*, pages 1–7, 2016.

[22] Joint Authorities for Rulemaking of Unmanned Systems. JARUS guidelines on Specific Operations Risk Assessment (SORA). Technical report, Edition 2.0, 2019.

[23] J.L. Kepert. The use of wreckage trajectories in aircraft accident investigation. Technical report, Defence Science and Technology Organization Aeronautical Research Laboratories, Melbourne, may 1976.

[24] David W. King, Allen Bertapelle, and Chad Moses. UAV Failure Rate Criteria for Equivalent Level of Safety. In *International Helicopter Safety Symposium*, page 9, Montreal, 2005.

[25] Anders la Cour-Harbo. Quantifying risk of ground impact fatalities of power line inspection BVLOS flight with small unmanned aircraft. In *2017 International Conference on Unmanned Aircraft Systems (ICUAS)*, pages 1352–1360, 2017.

[26] Xunguo Lin, Neale L. Fulton, and Mark E T Horn. Quantification of high level safety criteria for civil unmanned aircraft systems. In *IEEE Aerospace Conference Proceedings*, page 13, 2014.

[27] Lloyd's Register. Guidance Notes for Inspection using Unmanned Aircraft Systems. Technical report, mar 2016.

[28] Ministry of Transport and Building. Lov om ændring af lov om luftfart [Law on change of the law on aviation] - Law no. 602, 2016.

[29] NTSB. Trajectory study - Docket no. SA-516. Technical report, National Transportation Safety Board, 1997.

[30] Hugh E. Oldham. Aircraft debris trajectory analysis, 1990.

[31] R Frank Rabouw. Living near an Airport, Risky or just Annoying? Technical report, Delft University of Technology, 2000.

[32] R Frank Rabouw, Kimberly M Thompson, and Roger M Cooke. The Aviation Risk to Groundlings with Spatial Variability. In *Proceedings of ESREL*, page 8, 2001.

[33] Safety and Airspace Regulation Group Unmanned. Unmanned Aircraft System Operations in UK Airspace - Guidance - CAP 722. 6th Edition, 2015.

[34] Kimberly M Thompson, R Frank Rabouw, and Roger M Cooke. The Risk of Groundling Fatalities from Unintentional Airplane Crashes. *Risk Analysis*, 21(6):1025–1037, 2001.

[35] L A Twisdale and P J Vickery. Comparison of debris trajectory models for explosive safety hazard analysis. In *25th DoD Explosive Safety Seminar Anaheim, California*, pages 513–526, 1992.

[36] R. D. H Warburton, J. Wang, and J. Burgdörfer. Analytic approximations of projectile motion with quadratic air resistance. *Journal of Service Science & Management*, 2010(3):98–105, 2010.

[37] Michael Warren, Luis Mejias, Jonathan Kok, Xilin Yang, Felipe Gonzalez, and Ben Upcroft. An Automated Emergency Landing System for Fixed-Wing Aircraft: Planning and Control. *Journal of Field Robotics*, 32(8):1114–1140, dec 2015.

[38] Michael Warren, Luis Mejias, Xilin Yang, Bilal Arain, Felipe Gonzalez, and Ben Upcroft. Enabling Aircraft Emergency Landings Using Active Visual Site Detection. In *Field and Service Robotics*, pages 167–181. Springer Tracts in Advanced Robotics 105, 2015.

[39] D C Washington and 20594. In-flight Breakup Over the Atlantic Ocean Trans World Airlines Flight 800 Boeing 747-131, N93119 Near East Moriches, New York. Technical report, National Transportation Safety Board, 1996.

[40] Paul Wu and Reece Clothier. The Development of Ground Impact Models for the Analysis of the Risks Associated with Unmanned Aircraft Operations Over Inhabited Areas. In *Proceedings of the 11th Probabilistic Safety Assessment and Management Conference (PSAM11) and the Annual European Safety and Reliability Conference (ESREL 2012)*, page 14, 2012.